Unprecedented pressure increase in deep magma reservoir triggered by lava-dome collapse

B. Voight,[1] A. T. Linde,[2] I. S. Sacks,[2] G. S. Mattioli,[3] R. S. J. Sparks,[4] D. Elsworth,[1]
D. Hidayat,[1] P. E. Malin,[5] E. Shalev,[5] C. Widiwijayanti,[1] S. R. Young,[1] V. Bass,[6]
A. Clarke,[7] P. Dunkley,[6] W. Johnston,[3] N. McWhorter,[2] J. Neuberg,[8] and P. Williams[6]

[1] The collapse of the Soufrière Hills Volcano lava dome on Montserrat in July 2003 is the largest such event worldwide in the historical record. Here we report on borehole dilatometer data recording a remarkable and unprecedented rapid ($\sim$600s) pressurisation of a magma chamber, triggered by this surface collapse. The chamber expansion is indicated by an expansive offset at the near dilatometer sites coupled with contraction at the far site. By analyzing the strain data and using added constraints from experimental petrology and long-term edifice deformation from GPS geodesy, we prefer a source centered at approximately 6 km depth below the crater for an oblate spheroid with overpressure increase of order 1 MPa and average radius $\sim$1 km. Pressurisation is attributed to growth of 1–3% of gas bubbles in supersaturated magma, triggered by the dynamics of surface unloading. Recent simulations demonstrate that pressure recovery from bubble growth can exceed initial pressure drop by nearly an order of magnitude. **Citation:** Voight, B., et al. (2006), Unprecedented pressure increase in deep magma reservoir triggered by lava-dome collapse, *Geophys. Res. Lett.*, *33*, L03312, doi:10.1029/2005GL024870.

1. Introduction

[2] Data were obtained from the *Caribbean Andesite Lava Island Precision Seismo-geodetic Observatory, CALIPSO,* which investigates the dynamics of the Soufrière Hills Volcano (SHV) magmatic system by an integrated array of specialized instruments in four strategically located $\sim$200m-deep boreholes in concert with several shallower holes and surface instrumentation. Each borehole site (Figure 1) includes a very broad-band Sacks-Evertson dilatometer, a three-component seismometer, a tiltmeter, and a surface cGPS station [*Mattioli et al.*, 2004].

[3] The current eruption of SHV began in July 1995, and has been characterized by pulsatory extrusions and occasional explosions, resulting in $\sim$0.5 km^3 of andesitic lava erupted [*Druitt and Kokelaar*, 2002; *Voight et al.*, 1999]. The lava dome had been growing since the large collapse of July 2001 (Figure 2). The 2003 collapse started in the morning of 12 July and peaked between 02:30–05:30 UTC July 13. The volume lost from the dome is estimated as 210×10^6 m^3, with $\sim$17 $\times$ 10^6 m^3 and 5 $\times$ 10^6 m^3 eroded from Tar River Valley (TRV) and the shoreline fan, respectively [*Edmonds and Herd*, 2005]. Depressurisation triggered an explosion $\sim$03:35 UTC July 13 [*Edmonds and Herd*, 2005] and the seismic signal from the continuing collapse declined to background levels by $\sim$10:00 UTC 13 July. The eruption signals were recorded by three *CALIPSO* dilatometers and two borehole seismometers, and other surface instruments.

2. Analysis of Strain Signals

[4] Figure 3 shows low-pass (1000s) data for AIRS, TRNT, and GRLD sites. The overall shape of the volumetric strain offset, with some superposed broad "steps," and $\sim$20 min period oscillations, are relatively coherent at all sites. We emphasize the coherence of the strain patterns by reversing the GRLD trace and overlying it on the more proximal observations from AIRS and TRNT. The several steps in the strain offset correlate with individual clusters of surface collapse events manifested as peaks on the broadband seismic amplitude envelope, with a time lag of $\sim$10–15 min.

[5] Our most significant result is that the near sites (AIRS, TRNT) undergo expansion while the far site (GRLD) experiences contraction; these data are indicative of a deep-source volume expansion. The pressure in the magma chamber includes contributions from the ambient lithostatic load, an overpressure (in excess of lithostatic) caused by continual injection of deeper new magma, and pressurization processes in a gas-saturated and crystallizing magma body [*Tait et al.*, 1989; *Linde et al.*, 1994].

[6] The dome collapse reduced the mean lithostatic pressure in the rock-mass surrounding the chamber and caused a volumetric expansion of the chamber; the chamber overpressure increased and created strains detected by the dilatometer array. Our strain data can be evaluated to determine the depth of the pressure source, based on the radial distance where the volumetric strains at the $\sim$200 m dilatometer depth change polarity. For a deep, spherical source in an isotropic, homogeneous, elastic halfspace [*McTigue*, 1987], the depth relation is given by, radial

[1]College of Earth and Mineral Sciences, Pennsylvania State University, University Park, Pennsylvania, USA.

[2]Department of Terrestrial Magnetism, Carnegie Institution Washington, Washington, D. C., USA.

[3]Department of Geosciences, University of Arkansas, Fayetteville, Arkansas, USA.

[4]Department of Earth Sciences, Bristol University, Bristol, UK.

[5]Division of Earth and Ocean Sciences, Duke University, Durham, North Carolina, USA.

[6]Montserrat Volcano Observatory, Flemings, Montserrat, BWI.

[7]Geosciences, Arizona State University, Tempe, Arizona, USA.

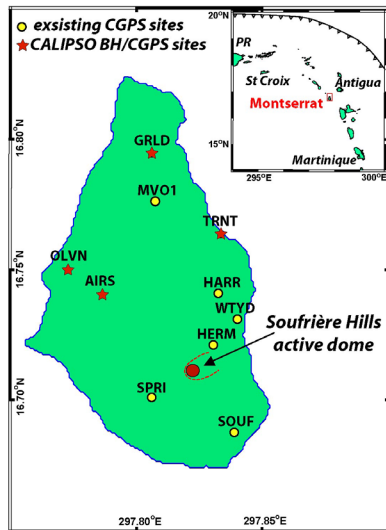[8]School of Earth Sciences, Leeds University, Leeds, UK.

Sudden pressure increase in magma reservoir triggered by gigantic lava dome collapse on Montserrat • History of the Martian dynamo • The Arctic influences subpolar wind patterns and European climate

Figure 1. Montserrat map showing location of CALIPSO boreholes and CGPS sites. Names of the sites referred to in the text are shown. Surface broadband seismometers are co-located at AIRS and HARR locations. A map of the northeastern Caribbean is inset.

distance = 1.4 * depth [*Linde and Sacks*, 1995]. For other source geometries, the polarity change occurs at different radial distances, e.g., for oblate ellipsoids (squashed spheres), the depth factor is around $1.0-1.2$ depending on aspect ratio. The volumetric strain generated by a spherical source is [*McTigue*, 1987; *Delaney and McTigue*, 1994]:

$$\varepsilon = (1 - 2\nu)\frac{\Delta P}{G}\left(\frac{a}{d}\right)^3 \frac{2(1 - z/d)^2 - (\rho/d)^2}{\left[(1 - z/d)^2 + (\rho/d)^2\right]^{3/2}}$$

where ν is Poisson's ratio (taken as 0.25), ΔP is the source pressure change, G is the elastic shear modulus, a is the source radius, d is depth to the center of the source, ρ and z are cylindrical polar coordinates with origin on the free surface centred over the pressure source and z positive upward. Radial displacement of the wall is $U_r = 0.25a(\Delta P/G)$ [*McTigue*, 1987]. Rock-mass modulus is known from barometer/strainmeter calibrations as well as the co-collapse elastic uplift observed at the HERM cGPS site ($\sim$0.02 m), and is estimated at $E \sim$10 GPa ($G = 4$ GPa). Other uncertainties relate to the unknown structural setting of the edifice, the effect of heterogeneous elastic constants, and the role of topography. The first is poorly constrained, and despite the good radial fit of the strain data from multiple azimuths, we cannot exclude the possibility of an effect from 3D asymmetry of magma chamber shape. Heterogeneity is also poorly constrained, but *De Natale and Pingue* [1996] conclude that for practical purposes the assumption of a homogeneous elastic medium is generally justified. Topography at Montserrat appears to have only a minor influence on far-field deformation [*Widiwijayanti et al.*, 2005].

[7] The calibrated CALIPSO dilatometer array enables ε to be measured at three sites. The derived values are +125, +100, and -70 nanostrain for AIRS, TRNT, GRLD, respectively, for the period of collapse from 01:12–


Figure 2. (a) Photo of the growing SHV lava dome taken in May 2003. View to W. Dome apex was over 1100 m AMSL at this time (D. Lea photo). (b) Photo from same location taken in August, 2003. Approximately 210 M m^3 of the dome collapsed within a 24 hr period starting July 12, 2003 (B. Voight photo).

04:50 UTC 13 July. These strains are adjusted for the elastic strain components resulting from removal of the vertical load within this time period (166 $\times$ 10^6 m^3 from dome (mixed lava and talus) at assumed average density $\sim$2100 kg/m^3, plus 17 $\times$ 10^6 m^3 at density $\sim$1900 kg/m^3 for fragmental deposits from the Tar River valley, with the material eroded at the fan cancelled by nearby deposition), and for deposition of most of the collapsed mass to distances between 2 and 7 km offshore. Similar densities were used by *Calder et al.* [2002]. These observations were used to correct our strain data. At AIRS, tephra deposits included 5 cm co-pyroclastic flow (PF) ash ($\sim$4 cm falling pre-01:12 UTC), 6 cm explosion + co-PF ash, and $2-3$ cm post-04:50 co-PF ash [*Edmonds and Herd*, 2005]; deposition was negligible at other sites. The large post-04:50 strain
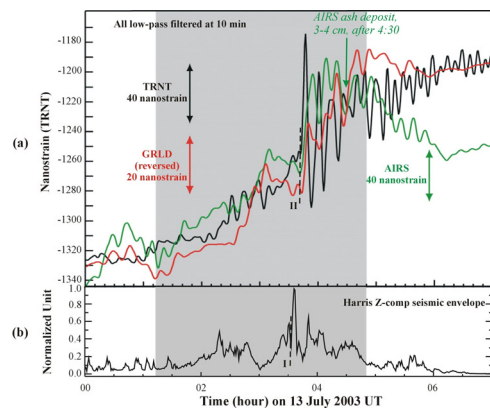
Figure 3. (a) Dilatometer records from the July 12–13, 2003 dome collapse as recorded at the AIRS, TRNT, and GRLD sites. The time scale is in hours with zero at 13/7/03 00:00 UT. (b) vertical component of seismic activity recorded at HAR broadband site, represented as seismic envelope. The shaded region marks the selected time window for pressure source analysis (see text). Note delay between seismic and dilatometer records as shown by the dashed lines I and II. Our focus here is the offset in strain during the interval between 00:00 and 04:30 hours. Other important information, to be considered elsewhere, includes the oscillatory ($\sim$20 min period) signals and strains due to surface load changes (e.g., post 04:30 ash load on AIRS produces negative (contraction) strain).
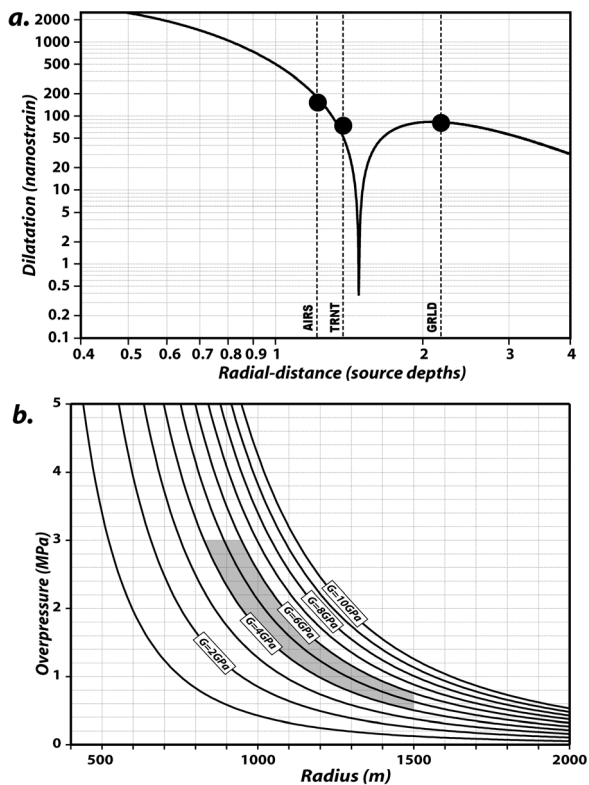
Figure 4. (a) Dilatational strain against radial distance, normalized as function of depth. Data indicate fits to data for July 2003 event. (b) Radius vs overpressure, for a range of shear moduli, consistent with data of Figure 4a. Shaded region denotes preferred data range.

changes at AIRS, ∼ 40 nanostrains, mainly reflect ash accumulation. The adjusted strains are +152, +74, and −81 nanostrains at the three sites.

3. Constraints on Source Parameters

[8] Plotting strains against radial distance from the vent allows the polarity reversal position (zero dilatation) to be determined, which then fixes the centroid depth for a spherical pressure source at 4.3 km below mean strainmeter elevation at −90 m elevation (∼5.1 km below the pre-eruption crater) (Figure 4). Alternatively for an ellipsoidal source with vertical-horizontal axis ratios of say 0.7, 0.6, 0.5 analytical solutions yield depths of 5.3, 5.9, and 6.3 km, respectively, and with extreme (unlikely) flattening, a limiting depth of ∼7.5 km. The latter depth estimates are consistent with petrological data [*Murphy et al.*, 2000; *Devine et al.*, 2003], phase equilibria constraints [*Barclay et al.*, 1998; *Rutherford and Devine*, 2003], seismological observations [*Aspinall et al.*, 1998], and surface deformation from GPS geodesy [*Mattioli et al.*, 1998]. The source region likely consists of a very crystal-rich magma which has been reheated and remobilized by repeated influx of mafic magma; the melt fraction in the reservoir is about 35–40%, the temperature is ∼830–860°C, and the rhyolitic melt is water saturated at 4.3–5 wt% at pressures of ∼130 MPa [*Barclay et al.*, 1998; *Murphy et al.*, 2000; *Devine et al.*, 2003; *Rutherford and Devine*, 2003]. It is

unlikely that any erupted magma was held for any extended time at a pressure less than the 130 MPa of phenocryst-melt equilibrium (5–6 km), otherwise hornblende reaction rims would exist on every grain [*Rutherford and Devine*, 2003]. The spherical model gives a depth for the *top* of the chamber that is slightly low to give pressures in the hornblende stability field and so a slightly flattened ellipsoid source is favored at a centroid depth of roughly 6 km, with an average radius of order 1 km. Depth estimates from the strain data depend somewhat on crustal structure (we have used a uniform half-space) but more important here are that these data are consistent with chemical signatures (independent of model details) and, surprisingly, that the reservoir experiences a pressure increase during dome collapse.

[9] Source centroid depth and vertical radii needed to fit petrologic and other constraints only weakly constrain source volume, i.e., $a <\sim$ 1.5 km. We note that ∼0.5 km^3 has been erupted with relatively steady flux rates over 8 years, which suggests the reservoir is "large" in comparison to lava output, $a \gg$ 0.5 km. Figure 4b shows the average chamber radius plotted against overpressure for variable G. The shaded area for G = 4–6 GPa and a = 0.85–1.5 km imply a ΔP = 0.5–3 MPa (with hot tensile strength ∼3 MPa, constraining the minimum size). An oblate ellipsoid (axial ratio 0.6) with ∼0.7 km vertical and ∼1.2 km horizontal radii also fit the data and is equivalent in volume to a sphere with 1 km radius, ∼4 km^3. The recently proposed SEA-CALIPSO seismic tomography and flow dynamic modelling experiment should additionally constrain chamber volume as well as shape [*Voight et al.*, 2005].

[10] The volume change caused by displacement of chamber walls is ∼$\pi(\Delta P/G)a^3$, giving for a ∼1 km, ∼2.6×10^5 to 2.4×10^6 m^3 for G in range 4–6 GPa. This change occurs within 1.3×10^4 s, implying an expansion rate of 20–180 m^3/s; this rate much exceeds the estimated magma injection rate of ∼2 m^3/s, such that magma replenishment cannot keep pace with it. The inference is further supported by the initial rapid deflation observed at the HERM cGPS site during the first 20 min of the collapse event.

4. Discussion and Concluding Remarks

[11] We next explore the hypothesis that the observed increase in pressure is largely driven by gas under two different scenarios: (1) the magma contains pressurized bubbles that expand when the ambient pressure is instantaneously reduced; or (2) a supersaturated melt phase exsolves gas under quasi-static conditions. For (1), viscous retardation of bubble expansion responding to a pressure drop ΔP in an infinite melt has a characteristic time scale of $\mu/\Delta P$ where μ is the dynamic viscosity [*Barclay et al.*, 1995]. Taking 3×10^5 Pa.s as the estimated viscosity of the rhyolitic melt fraction of the partly crystalline andesite of the SHV at 850°C and 4.6 wt% dissolved water [*Dingwell et al.*, 1996], and a pressure drop of ∼0.1 MPa from Boussinesq relations [*Poulos and Davis*, 1974] for dome unloading, the time scale is of order one second and is independent of bubble size [*Barclay et al.*, 1995]. Using 170 kg/m^3 for the density of water vapour under these conditions, volume expansion in the range 3–8×10^5 m^3 can be accommodated with volume fractions of bubble of 1–3%. Note that

bubbles may not be uniformly distributed throughout the full chamber, but rather may be concentrated at shallow levels; if so, our modeling of a pressure source is relevant to only to this bubble-rich portion of the chamber. Recent simulations demonstrate that for conditions similar to those inferred at SHV, pressure recovery from bubble growth can exceed initial pressure drop (e.g., 0.1 MPa) by nearly an order of magnitude [*Nishimura*, 2004].

[12] For (2), gas exsolution is governed by diffusion, and we calculate from experimental data diffusivity D of water in rhyolite melt at 850°C with $\sim$4.6 wt% water as 4×10^{-11} m^2/s [*Zhang and Behrens*, 2000]. We next calculate the distance l over which diffusion can act in the observed time-scale $t = 600$ s from the relation $t = l^2/D$, giving $l = 150$ microns. To gain a fast diffusive response, bubbles need to be spaced at distances of this order. Using $\sim$3% bubbles as suggested above and assuming 60% crystallinity, the effective bubble fraction in the melt phase is 7.5%. For a bubble radius of 50 μm, the mean spacing distance is 90 μm, and the half-spacing 45 μm. If the bubbles are evenly spaced and each is imagined to fill a box, then the farthest distance from a bubble edge to melt in the corner of the box is also 90 μm. Thus it appears that water diffusion could yield a real magma pressure increase and produce a supersaturation pressure as observed by the strain data. The process might be aided by enhanced nucleation induced by seismo-mechanical dynamic agitation of the magma chamber by the dome collapse.

[13] Our preferred model mainly requires volumetric adjustment of pre-existing bubbles at SHV magma; this is consistent with observations that the volcano is discharging a much larger mass of SO$_2$ than can be dissolved in the magma chamber [*Edmonds et al.*, 2001; *Norton et al.*, 2002]. The enhanced overpressures of the magmatic system in July 2003 may also have contributed to the explosive eruptions that occurred at a late stage of collapse and shortly after the collapse. These results demonstrate that significant information on magmatic systems can be derived from strainmeter arrays, and should encourage their deployment at other volcanoes.

References

Aspinall, W. P., et al. (1998), Soufriere Hills eruption, Montserrat, 1995–1997: Volcanic earthquake locations and fault plane solutions, *Geophys. Res. Lett.*, 25, 3397–3400.

Barclay, J., D. S. Riley, and R. S. J. Sparks (1995), Analytical models for bubble growth during decompression of high viscosity magmas, *Bull. Volcanol.*, 57, 422–431.

Barclay, J., et al. (1998), Experimental phase equilibria constraints on pre-eruptive storage conditions of the Soufriere Hills magma, *Geophys. Res. Lett.*, 25, 3437–3440.

Calder, E. S., R. Luckett, R. S. J. Sparks, and B. Voight (2002), Mechanisms of lava dome instability and generation of rockfalls and pyroclastic flows at Soufriere Hills Volcano, Montserrat, *Geol. Soc. London Mem.*, 21, 173–190.

Delaney, P. T., and D. F. McTigue (1994), Volume of magma accumulation or withdrawal estimated from surface uplift or subsidence, with application to the 1960 collapse of Kilauea volcano, *Bull. Volcanol.*, 56, 417–424.

De Natale, G., and F. Pingue (1996), Ground deformation modelling in volcanic areas, in *Monitoring and Mitigation of Volcano Hazards*, edited by R. Scarpa and R. Tilling, pp. 365–388, Springer, New York.

Devine, J. D., et al. (2003), Magma storage region processes inferred from geochemistry of Fe-Ti oxides in andesitic magma, Soufriere Hills volcano, Montserrat, W.I., *J. Petrol.*, 44, 1375–1400.

Dingwell, D. B., C. Romano, and K. U. Hess (1996), The effect of water on the viscosity of haplogranitic melt under P-T-X conditions relative to silicic volcanism, *Contrib. Mineral. Petrol.*, 124, 19–28.

Druitt, T. H., and P. Kokelaar (Eds.) (2002), *The Eruption of Soufrière Hills Volcano, From 1995 to 1999*, Geol. Soc. London Mem., 21, 645 pp.

Edmonds, M., and R. Herd (2005), Inland-directed base surge generated by the explosive interaction of pyroclastic flows and seawater at Soufrière Hills volcano, Montserrat, *Geology*, 33, 245–248.

Edmonds, M., D. Pyle, and C. Oppenheimer (2001), A model for degassing at the Soufrière Hills Volcano, Montserrat, West Indies, based on geochemical data, *Earth Planet. Sci. Lett.*, 186, 159–173.

Linde, A. T., and L. S. Sacks (1995), Continuous monitoring of volcanoes with borehole strainmeters, in *Mauna Loa Revealed: Structure, Composition, History, and Hazards, Geophys. Monogr. Ser.*, vol. 92, edited by J. M. Rhodes and John P. Lockwood, pp. 171–185, AGU, Washington, D. C.

Linde, A. T., et al. (1994), Increased pressure from rising bubbles as a mechanism for remotely triggered seismicity, *Nature*, 371, 408–410.

Mattioli, G. S., T. H. Dixon, F. Farina, E. Howell, P. Jansma, and A. L. Smith (1998), GPS measurement of surface deformation around Soufriere Hills volcano, Montserrat from October 1995 to July 1996, *Geophys. Res. Lett.*, 25, 3417–3420.

Mattioli, G., et al. (2004), Prototype PBO instrumentation of CALIPSO Project captures world-record lava dome collapse on Montserrat, *Eos Trans. AGU*, 85(34), 317–325.

McTigue, D. F. (1987), Elastic stress and deformation near a finite spherical magma body: Resolution of the point source paradox, *J. Geophys. Res.*, 92, 12,931–12,940.

Murphy, M. D., et al. (2000), Remobilisation of andesite magma by intrusion of mafic magma at the Soufriere Hills volcano, Montserrat, *J. Petrol.*, 41, 21–42.

Nishimura, T. (2004), Pressure recovery in magma due to bubble growth, *Geophys. Res. Lett.*, 31, L12613, doi:10.1029/2004GL019810.

Norton, G. E., et al. (2002), Pyroclastic flow and explosive activity of the lava dome of Soufriere Hills volcano, Montserrat during a period of virtually no magma extrusion (March 1998 to November 1999), *Geol. Soc. London Mem.*, 21, 467–482.

Poulos, H. G., and E. H. Davis (1974), *Elastic Solutions for Soil and Rock Mechanics*, 411 pp., John Wiley, Hoboken, N. J.

Rutherford, M. J., and J. D. Devine (2003), Magmatic conditions and magma ascent as indicated by hornblende phase equilibria and reactions in the 1995–2002 Soufrière Hills magma, *J. Petrol.*, 44, 1433–1454.

Tait, S. R., C. Jaupart, and S. Vergniolle (1989), Pressure, gas content and eruption periodicity in a shallow crystallising magma chamber, *Earth Planet. Sci. Lett.*, 92, 107–123.

Voight, B., et al. (1999), Magma flow instability and cyclic activity at Soufrière Hills volcano, Montserrat, British West Indies, *Science*, 283, 1138–1142.

Voight, B., et al. (2005), SEA-CALIPSO "Onshore-Offshore" Seismic Experiment to image Magma Reservoir on Montserrat, paper presented at "Soufriere Hills Volcano—Ten Years On" Conference, Seismic Res. Unit, Univ. of the W. Indies, Montserrat.

Widiwijayanti, C., A. Clarke, D. Elsworth, and B. Voight (2005), Geodetic constraints on the shallow magma system at Soufrière Hills volcano, Montserrat, *Geophys. Res. Lett.*, 32, L11309, doi:10.1029/2005GL022846.

Zhang, Y., and H. Behrens (2000), H$_2$O diffusion in rhyolitic melts and glasses, *Chem. Geol.*, 169, 243–262.

V. Bass, P. Dunkley, and P. Williams, Montserrat Volcano Observatory, Flemings, Montserrat, BWI.

A. Clarke, Geosciences, Arizona State University, Tempe, AZ 85287, USA.

D. Elsworth, D. Hidayat, B. Voight, C. Widiwijayanti, and S. R. Young, College of Earth and Mineral Sciences, Pennsylvania State University, University Park, PA 16802-2714, USA. (voight@ems.psu.edu)

W. Johnston and G. S. Mattioli, Department of Geosciences, University of Arkansas, Fayetteville, AR 72701, USA.

A. T. Linde, N. McWhorter, and I. S. Sacks, Department of Terrestrial Magnetism, Carnegie Institution Washington, Washington, DC 20015-1305, USA.

P. E. Malin and E. Shalev, Division of Earth and Ocean Sciences, Duke University, Durham, NC 27708-0235, USA.

J. Neuberg, School of Earth Sciences, Leeds University, Leeds, LS2 9JT, UK.

R. S. J. Sparks, Department of Earth Sciences, Bristol University, Bristol BS8 1RJ, UK.